NASA Technical Memorandum 102471

An Analysis of the Viscous Flow Through a Compact Radial Turbine by the Average Passage Approach

James D. Heidmann
Lewis Research Center
Cleveland, Ohio

and

Timothy A. Beach
Sverdrup Technology, Inc.
NASA Lewis Research Center Group
Cleveland, Ohio

NASA

AN ANALYSIS OF THE VISCOUS FLOW THROUGH A COMPACT RADIAL TURBINE BY THE AVERAGE PASSAGE APPROACH

James D. Heidmann
National Aeronautics and Space Administration
Lewis Research Center
Cleveland, Ohio 44135 USA

and

Timothy A. Beach
Sverdrup Technology, Inc.
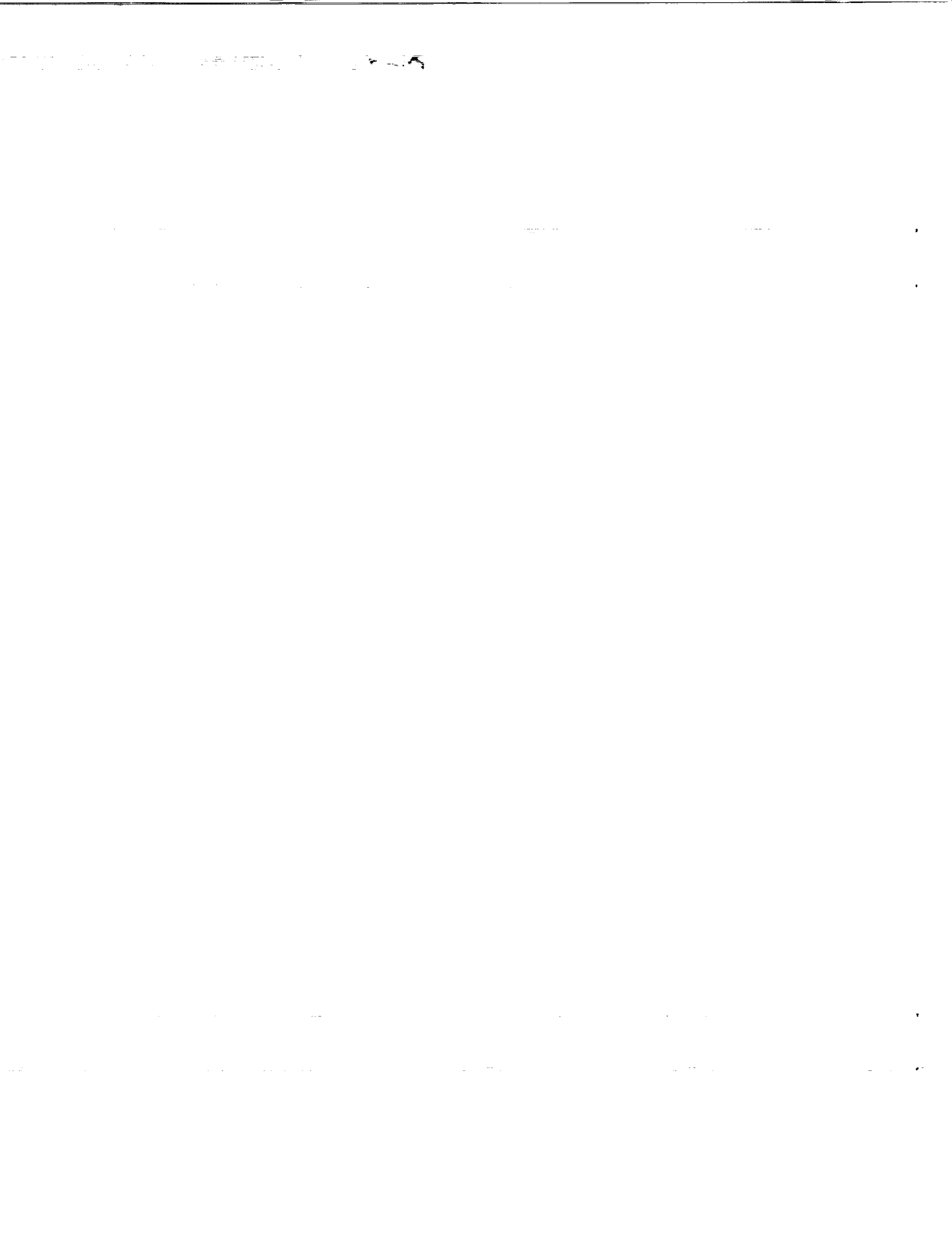NASA Lewis Research Center Group
Cleveland, Ohio 44135

ABSTRACT

A steady, three-dimensional viscous "average passage" computer code is used to analyze the flow through a compact radial turbine rotor. The code models the flow as spatially periodic from blade passage to blade passage. Results from the code using varying computational models are compared with each other and with experimental data. These results include blade surface velocities and pressures, exit vorticity and entropy contour plots, shroud pressures, and spanwise exit total temperature, total pressure, and swirl distributions. The three computational models used are inviscid, viscous with no blade clearance, and viscous with blade clearance. It is found that modeling viscous effects improves correlation with experimental data, while modeling hub and tip clearances further improves some comparisons. Experimental results such as a local maximum of exit swirl, reduced exit total pressures at the walls, and exit total temperature magnitudes are explained by interpretation of the flow physics and computed secondary flows. Trends in the computed blade loading diagrams are similarly explained.

INTRODUCTION

The use of radial turbines is advantageous in small propulsion engines due to high efficiencies and the large pressure ratios achievable in one stage. Furthermore, the use of only one radial turbine stage in place of several axial turbine stages can improve reliability through reduced part count. However, the size and weight of present radial turbine rotor designs makes them undesirable for future advanced aircraft applications. In addition, low cycle fatigue life is a major concern for man-rated applications based on present radial rotor sizes and anticipated future tip speeds. A compact radial turbine which is 40 to 50 percent shorter in axial length, 4 percent smaller in diameter, and 20 to 30 percent lighter than current state-of-the-art radial turbines has been designed and fabricated by Pratt and Whitney and tested at NASA Lewis Research Center.

In an effort to understand the complex flow physics associated with the compact radial turbine rotor operation and to help explain experimental data, a computational study of the rotor flow field was undertaken. A fully three-dimensional code is desired because of the highly complex flow associated with radial turbine flow. This is especially true for the compact radial turbine owing to the short axial distance over which the flow is turned. Previous three-dimensional computational study of radial turbines is sparse, but Choo and Civinskas (Ref. 1) reported a three-dimensional inviscid analysis of a radial turbine flow using the DENTON code (Ref. 2). Viscous effects such as boundary layer separation and wake development were cited as possible causes of predicted underturning relative to experimental exit flow angles. Zangeneh-Kazemi et al. (Ref. 3) conducted a three-dimensional viscous analysis of a radial turbine and compared the results with experimental data. It was recommended that a tip clearance model be incorporated for accurate simulation of radial turbine flow fields. Good agreement was found between experimental and computed results, especially for the calculation accounting for tip clearance. However, it is difficult to interpret the comparisons from a turbine design standpoint due to the lack of axisymmetric average comparisons. In addition, no inviscid results are presented for comparison to the more accurate models. The present study aims to produce comparisons with experimental data by considering axisymmetric average quantities. Comparisons are also made in the present study between three solutions of increasing physical realism: inviscid, viscous with no blade clearance, and viscous with blade clearance. Such comparisons are needed to ultimately extend the use of three-dimensional viscous turbomachinery codes to the turbine design field, because in this way the inaccuracies of the inviscid and nonclearance assumptions can be isolated and analyzed.

In the present study, a three-dimensional viscous computer code of Adamczyk (Refs. 4 to 6) is used. This code is an "average passage" code which models the flow as spatially periodic from blade passage to blade passage in a particular blade row and can be used to model

multiple blade rows. This is particularly advantageous in multistage turbomachinery calculations, where this averaging process keeps computational time from becoming prohibitive. For a single blade row, the code is essentially identical to a fully three-dimensional viscous code. A tip clearance model is included in the analysis, as recommended by Zangeneh-Kazemi et al. In addition, a blade hub clearance model is included which models the backface clearance typically found in radial turbine rotors.

ROTOR DESCRIPTION

The compact radial turbine rotor is shown in Fig. 1. The rotor has 14 solid blades attached to a solid disk. The rotor has radial inflow and axial outflow and is scalloped; that is, the disk does not extend to the leading edge of the blades. Instead, the flow is bounded by the stationary backface in this region. Likewise, the stationary aft centerbody is in contact with the flow downstream of the rotor. Figure 2 details the relevant rotor features. The shroud clearance is about 0.046 cm (0.018 in.) at the leading edge and 0.020 cm (0.008 in.) at the trailing edge. The backface clearance is about 0.038 cm (0.015 in.). The rotor diameter is 0.367 m (14.5 in.) to the blade leading edge.

Figure 3 illustrates the 40 percent reduction in axial length achieved with the compact radial turbine design compared to a state-of-the-art radial turbine of the same class. The reduction in length holds several advantages. In addition to the size and weight reductions important for aircraft applications, a shorter rotor reduces the unsupported shaft length between bearings, resulting in improved rotor dynamics.

The experimental study of the compact radial turbine was conducted in the NASA Lewis Warm Turbine Test Facility under a joint program with Pratt and Whitney. Due to the confidential nature of the program, this data has not been fully published and disclosure of turbine efficiencies is restricted. Preliminary testing consisted of a tare test on the basic rig with a
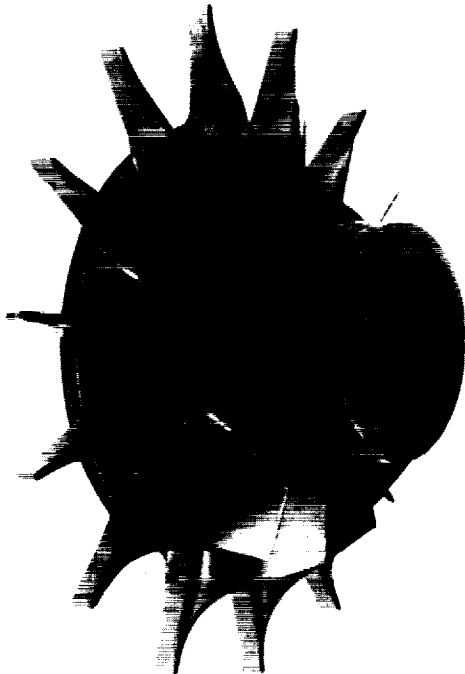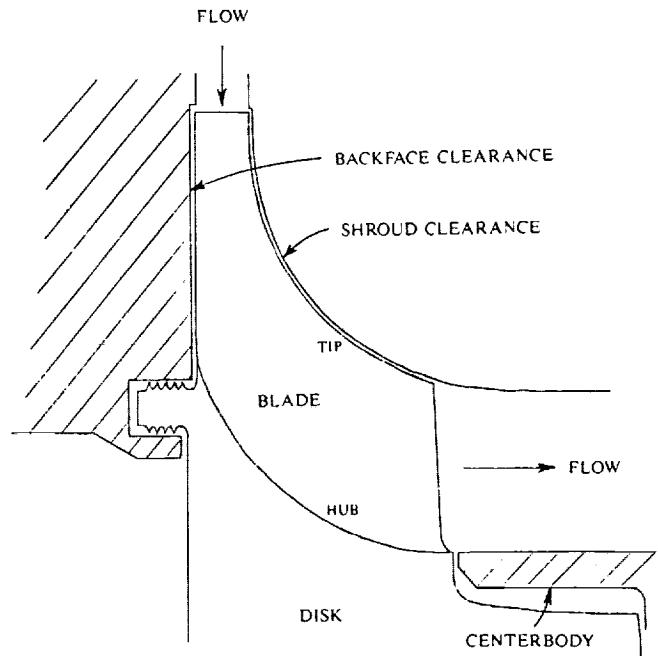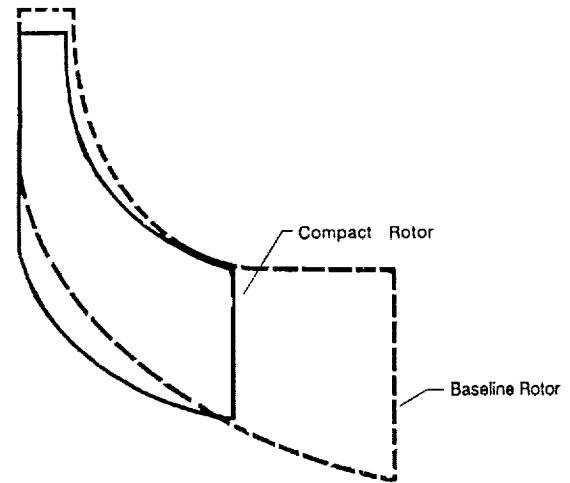

Figure 2 - Rotor assembly

Figure 3 - Compact rotor profile comparison

bladeless rotor. This was done to measure the losses associated with the rig itself; namely windage, bearing, and seal losses. Next, the rotor was installed into the rig, and testing was conducted over a matrix of test conditions. This matrix consisted of a range of pressure ratios and rotor speeds centered about the design point. The design point for the turbine was 20 000 rpm, 5.0 pressure ratio, 2.86 kg/s (6.30 lb/s) flow rate, and 478 K (860 °R) rotor total inlet temperature. This corresponds to a Reynolds number of 1.90×10^{7} based on rotor diameter and inlet conditions. Rotor exit surveys were conducted which measured flow angles, total temperatures, and total pressures versus percent span. In addition, shroud static pressures were recorded versus meridional distance. All data was recorded at a steady-state condition. The design point data from these experiments is used for comparison to calculation in this report.

Figure 1 - Compact radial rotor

2

CODE DESCRIPTION

The code used to analyze the compact radial turbine is a three-dimensional viscous "average passage" code (Refs. 4 to 6). The code uses three averaging processes to obtain the average passage equations from the full Navier-Stokes equations. These are ensemble averaging, time averaging, and passage-to-passage averaging. Ensemble averaging yields the familiar Reynolds-averaged Navier-Stokes equations. This averaging process removes the random fluctuations from the flow field. Time averaging further simplifies the flow equations by removing the deterministic unsteady flow component which occurs because of the relative movement of different blade rows. Finally, the equations are passage-to-passage averaged, which removes the effect of different blade count of stator and/or rotor blade rows. In this procedure, the flow is assumed to be spatially periodic from blade passage to blade passage in a particular blade row. For multistage turbomachinery, with stator blade rows and/or rotor blade rows having different numbers of blades, this will not generally be true. The average passage equations obtained by the three averaging processes are discretized using a control volume approach in a cylindrical coordinate system. Using this control volume approach, all flow quantities are cell-centered. To obtain values of flow variables at cell surfaces, an averaging process is used which results in second-order accuracy. In the viscous solutions, a Baldwin-Lomax turbulence model is employed. The turbulence model is updated after every 10 iterations.

The discretized average passage equations obtained by the control volume approach are solved using a four-stage Runge-Kutta scheme. Second and fourth difference smoothing operators are used to avoid alternate point decoupling in the solution. The Riemann invariants C^+ and C^- are used to calculate the radial velocity component at the upstream boundary. Constant entropy is assumed from an upstream state to the inlet boundary, and this is used to determine the inflow temperature, pressure, and density. At the downstream boundary, the static pressure at the hub is specified and radial equilibrium is enforced across the span. All other downstream flow quantities are extrapolated from the interior of the flow domain. At the blade, hub, and shroud surfaces, an extrapolated normal pressure gradient boundary condition is employed in conjunction with an adiabatic wall. The hub velocity boundary condition was adapted for the scalloped rotor configuration. In the viscous solutions, the computational cells which lie in the stationary backface and aft centerbody regions employ a zero velocity boundary condition. All other hub cells use the rotor speed as the velocity boundary condition, which is typical. The shroud is of course stationary in the absolute frame of reference and is so modeled. For the inviscid solution, the absence of viscous forces renders rotation of axisymmetric surfaces inconsequential. The mesh boundaries extending from the blade leading and trailing edges to the inflow and outflow boundaries, respectively, are periodic boundaries. At these boundaries, periodicity is enforced by setting the flow variables in the computational cell outside the computational domain equal to those at the corresponding periodic location.

The code contains a one-dimensional inviscid flow model for the clearance gap flow. This model conserves mass, momentum, and total enthalpy across the clearance gap. As a result, the pressure difference across the gap is zero. This is a rather simplified representation of the flow in the clearance region, but it does result in a flow across the clearance gap which serves to reduce the loading in the tip region. This model is simply implemented by enforcing the previously stated periodic boundary conditions. This model for the flow in the clearance gap was applied to the entire blade tip and to the hub backface clearance.

METHOD OF ANALYSIS

The average passage code was first modified for use with radial turbomachinery. Among these modifications was the changing of the upstream velocity boundary condition from axial to radial flow and the replacement of various axial velocity approximations by the true velocity. The code was then in an appropriate form to analyze the compact radial turbine rotor. Although the code is capable of analyzing the entire turbine stage, this was not done as part of this analysis. Instead, it was assumed that the flow upstream of the rotor was axisymmetric and spanwise constant. In a true three-dimensional stage calculation, neither of these assumptions would be made. The experimental inlet flow was not spanwise constant, since boundary layers formed on the hub and shroud surfaces. However, spanwise constancy was assumed in the calculation for simplicity.

A three-dimensional computational grid was generated for the rotor blade passage using an interactive H-grid generator. The hub and suction surface grid is shown in Fig. 4. The grid size is 109 by 33 by 33 grid points, with 109 grid points in the flow direction. The grid includes densely-packed grid points near the solid boundaries to adequately resolve viscous effects. The wall spacing is from 0.0025 to 0.0050 cm (0.0010 to 0.0020 in.) over most of the blade, hub, and shroud surfaces. The grid extends from about 13 percent of midspan chord upstream of the blade leading edge to about 27 percent of midspan chord downstream of the blade trailing edge. The midspan chord is defined as the arc length of the midspan grid line on the blade surface. Grid points are packed densely in the streamwise direction around the elliptic leading and trailing edges of the blades. This is necessary to adequately resolve the accelerating flow in these regions. The grid spacing for the first two grid points in the streamwise direction around the blade leading and trailing edges is about 0.011 cm (0.0043 in.). There are two grid points in the tip clearance region and three in the hub clearance region. Only one grid was employed in the calculations, so the effect of different grid densities could not be studied.

The code requires specification of upstream total temperature and pressure, upstream swirl velocity, downstream static pressure at the hub, and rotor speed. Downstream static pressure, upstream total temperature, and rotor speed were taken to match experimental conditions at the design point. The upstream swirl velocity was taken to match design conditions based on the stator exit blade angle. The upstream total pressure was calculated based on a 2 percent reduction from the stator inlet value. The mass flow rate is calculated by the code. A fuel-to-air ratio of 0.0042 was used to determine the gas constant of 288.1 m^2/s^2 K (1723 ft^2/s^2 °R). Since constant specific heats were assumed in the calculation, a mean value of 1.39 was used for the specific heat ratio.

A two-dimensional inviscid hub-to-shroud midchannel stream surface solution was obtained for the rotor flow field using the MERIDL code (Ref. 7). This solution was interpolated to the three-dimensional grid for use as a starting solution for the three-dimensional average passage calculation. Three solutions of the rotor flow field were made using varying computational models. The first solution employed the inviscid form of the code. The second solution employed the viscous turbulent form of the code. This solution attempted to
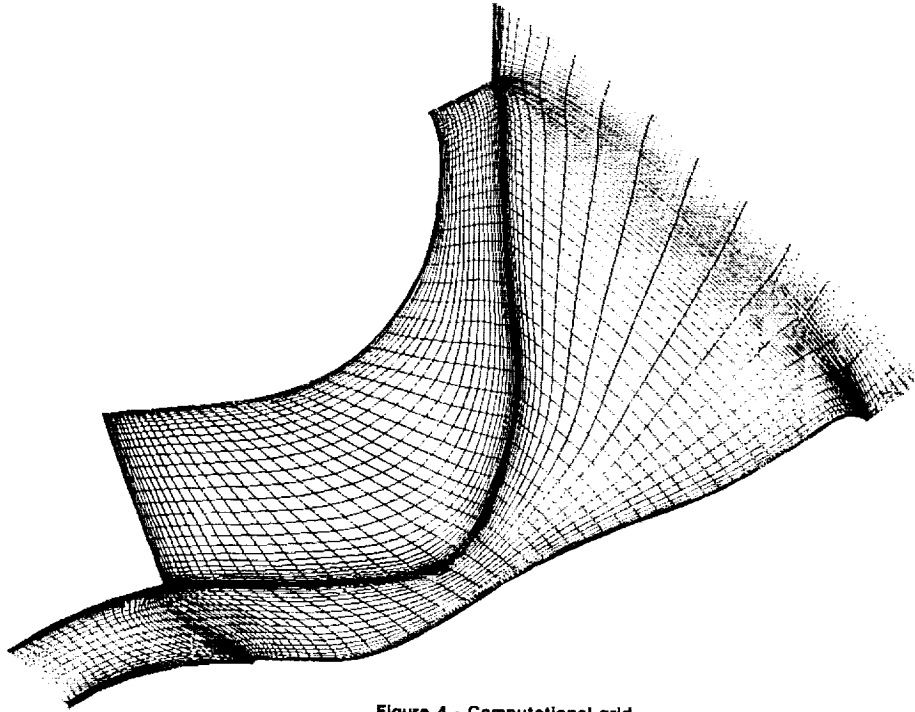
Figure 4 - Computational grid

accurately model the rotor backface and aft centerbody by specifying these regions as stationary. The third solution differed from the second solution only in that it included the effects of the hub and tip clearances. The hub clearance is due to the separation distance between the rotor backface and the blades in the radial portion of the rotor. All three solutions employed the same computational grid. The code was run for each of the three cases until the root-mean-square average of the residuals at each grid point had decreased by at least three orders of magnitude from the starting solution. The residual was defined as the time derivative of the gas density at a specific location.

The computations were performed on a CRAY-2 super-computer. The inviscid and viscous solutions required approximately 2000 and 4000 iterations, respectively, to reach a converged solution from a rough starting solution. This corresponds to approximately 1.75 and 4.25 CPU hours of run time, respectively. The computational grid, executable code, and flow solution required about 2.5 kiloblocks of combined memory.

RESULTS AND DISCUSSION

Figures 5 to 7 correspond to the viscous nonclear-ance solution. Figure 5 presents the relative velocity vectors at the grid points adjacent to the hub and blade suction surfaces. Over most of the blade suction surface, the spanwise component of the flow adjacent to the blade is directed toward the shroud. However, near the blade tip the flow vectors point away from the shroud. This is due to viscous effects at the shroud. In the rotating frame of reference, the fluid adjacent to the shroud is dragged by the shroud into the suction surface of the blade. This causes the flow near the shroud to curl into a counterclockwise vortex (as viewed from downstream) known as the scraping vortex. This scraping vortex is counter to the direction of the passage vortex. The clockwise passage vortex is pro-duced by the components of streamline curvature and Coriolis acceleration in the direction of absolute vor-ticity of the flow and is an inviscid effect. Figure 6

shows the counterrotating vortices in more detail. This is a contour plot of axial vorticity on the grid plane containing the blade trailing edges as viewed from a downstream viewpoint. The vorticity is non-dimensionalized by the ratio of reference velocity to reference length. The reference velocity is the stag-nation sonic velocity at the rotor inlet divided by the square root of the specific heat ratio and the refer-ence length is the rotor diameter. The blade suction surface is to the left of the figure. The vortices are adjacent to the suction surface near the shroud. It can be seen from the sense of rotation of the vortices that the fluid between them is driven away from the wall. This indicates that the boundary layer fluid on the suction surface is pulled away from the blade sur-face into the main flow by the vortices. Since the boundary layer flow contains high loss fluid, this vor-tex action brings higher loss fluid into the main flow. This is confirmed by Fig. 7, which is a plot of entropy on the same exit plane. The entropy is nondimensional-ized by the gas constant and the zero entropy datum is at the rotor inlet. The high entropy (high loss) flow is centered between the two counterrotating vortices. Figure 6 also shows regions of high vorticity along the blade pressure surface. This is associated with the origin of the viscous wake. Figure 7 establishes this region as high entropy, high loss flow.

The final converged solution for the viscous blade clearance model represents the most physically realis-tic model used in the analysis of the rotor. Figures 8 to 11 correspond to this solution. Figure 8 shows the relative velocity vectors at the grid points adjacent to the hub and blade suction surfaces. Over most of the blade suction surface, the spanwise component of the flow adjacent to the blade is directed toward the shroud. This effect is again due to the passage vortex which rotates in the clockwise direction. The vectors near the hub and tip which are in the circumferential direction represent the leakage flow in the blade clearance regions. This leakage flow reduces the effi-ciency of the machine since the fluid does no work on the blade.
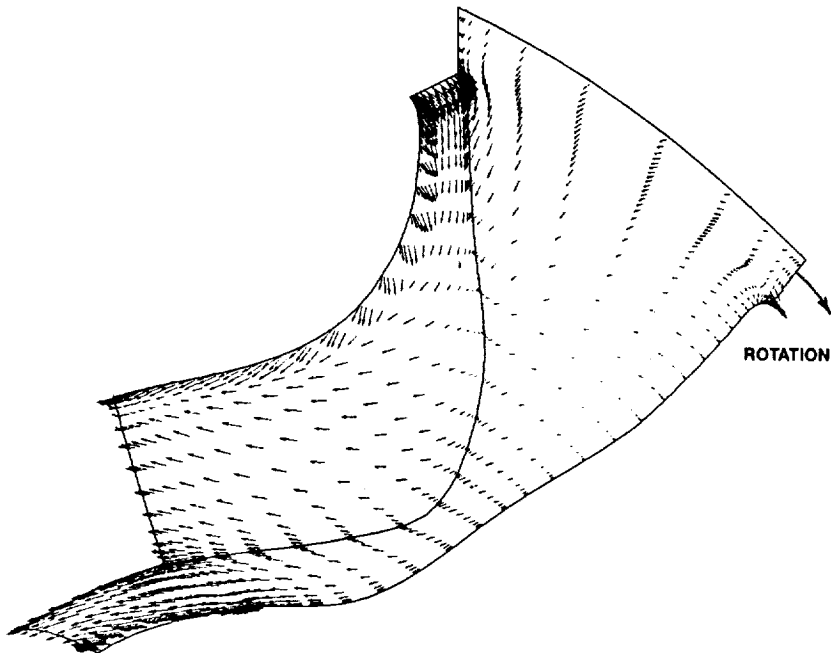
4

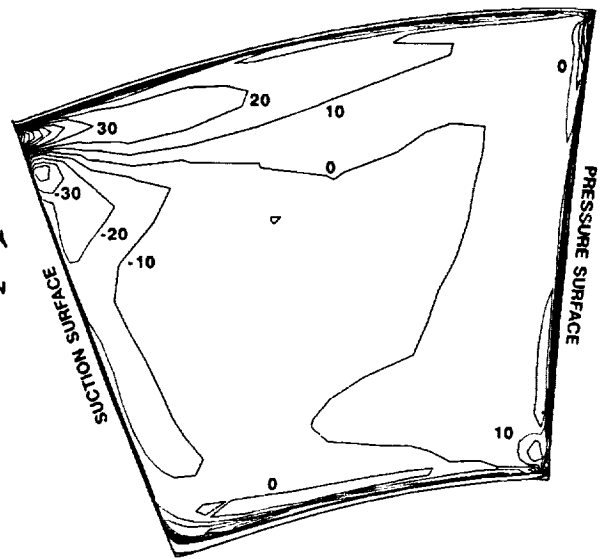**Figure 5 - Non-clearance viscous solution relative velocity vectors**

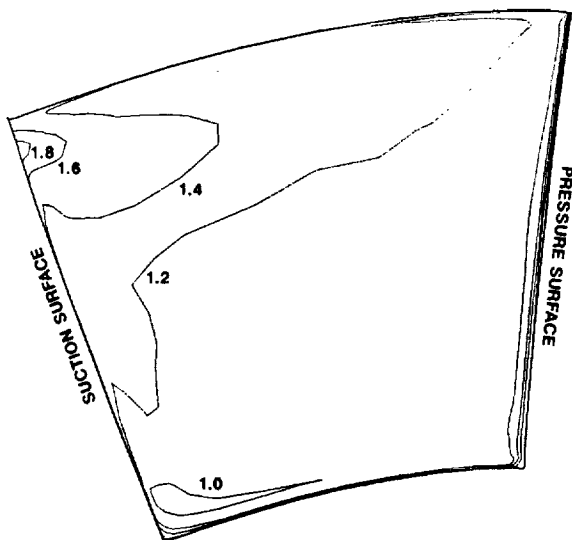**Figure 6 - Non-clearance viscous solution exit axial vorticity**

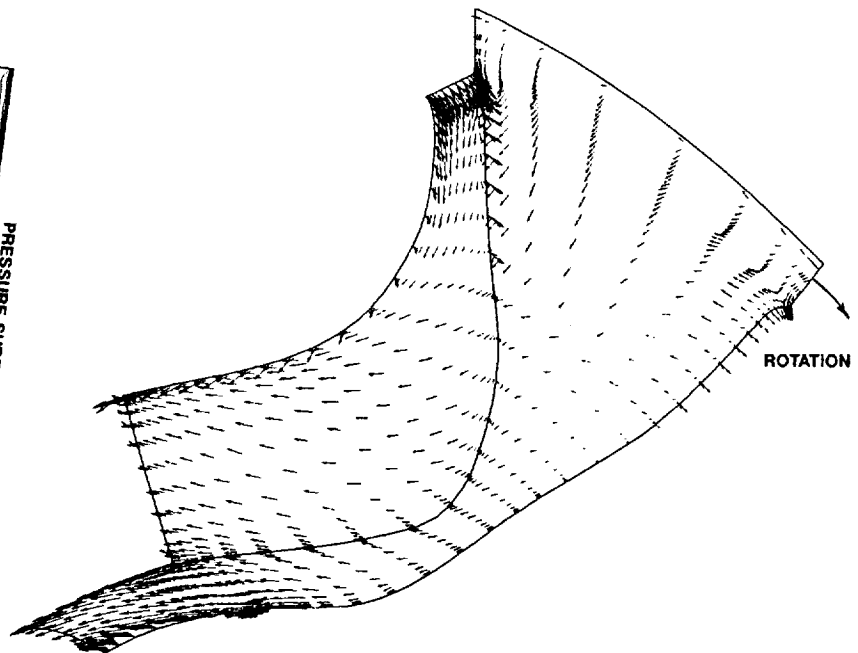**Figure 7 - Non-clearance viscous solution exit entropy**

Figure 8 - Clearance viscous solution relative velocity vectors

Figure 9 shows the axial component of vorticity on the grid plane containing the blade trailing edges. The vorticity is nondimensionalized by the ratio of reference velocity to reference length. The reference velocity is the stagnation sonic velocity at the rotor inlet divided by the square root of the specific heat ratio and the reference length is the rotor diameter. The tip clearance flow is driven by pressure differences from the pressure to the suction surface (left to right in Fig. 9) and causes the vorticity to be negative (clockwise) over most of the region near the suction tip corner. The counterrotating vortex pattern present in the nonclearance viscous solution is destroyed by the clearance flow. However, another mechanism causes loss in the clearance solution which is not present in the nonclearance solution. The high loss tip clearance flow passes over the blade tip along the entire length of the blade and penetrates into the flow along the shroud toward the adjacent blade. The high loss in the clearance flow is produced by viscous effects at the shroud. In the rotating frame of reference, the fluid very close to the shroud rotates with the shroud due to viscous effects. This causes the relative circumferential velocity very near the shroud to be in the opposite direction to the clearance flow. The resultant high shear region generates loss in the
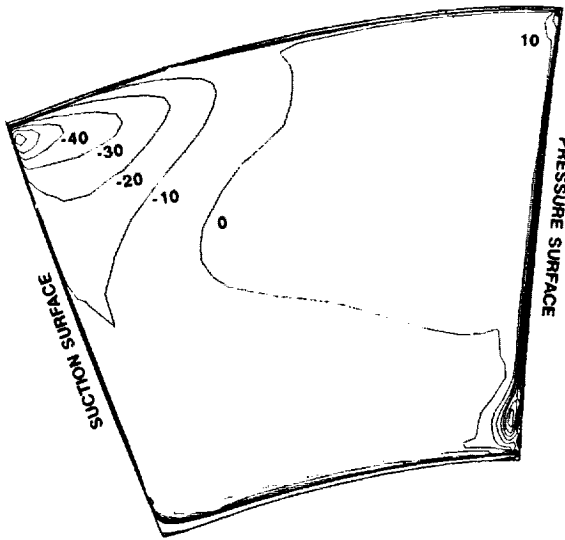
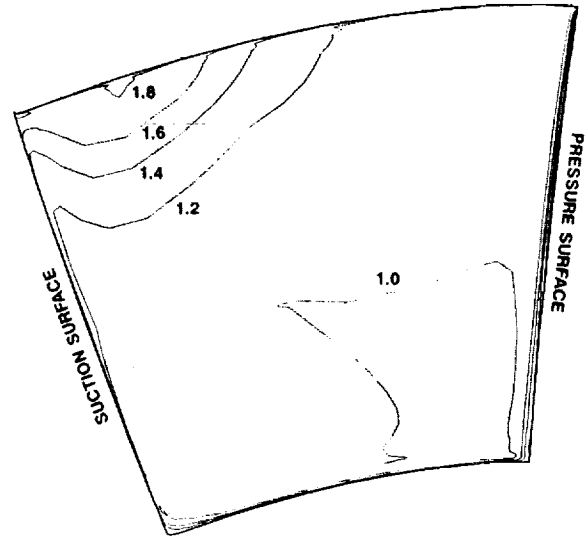Figure 9 - Clearance viscous solution exit axial vorticity

Figure 10 - Clearance viscous solution exit entropy

Figure 11 - Clearance viscous solution blade-to-
blade midspan critical velocity ratio

clearance flow as it travels along the shroud. This is
illustrated in Fig. 10, which is a plot of entropy on
the same exit plane as Fig. 9. The entropy is nondi-
mensionalized by the gas constant and the zero entropy
datum is at the rotor inlet. The high entropy region
adjacent to the shroud and slightly away from the suc-
tion surface is due to the high loss clearance flow
which accumulates in this region. Figure 9 indicates
regions of large vorticity near the blade pressure sur-
face, as was seen in Fig. 6 for the nonclearance vis-
cous solution. As previously noted, this corresponds
to the beginning of the turbulent wake, and is
reflected as increased entropy in Fig. 10.

It appears from Figs. 6, 7, 9, and 10 that the
boundary layer on the blade pressure surface is thicker
than that on the blade suction surface. These figures
are plotted on the grid plane containing the blade
trailing edges. From Fig. 4 it can be seen that this
plane is curved, particularly near the blades. This
curvature causes more of the grid plane to pass through
the blade aft wake on the pressure side. This is con-
firmed by Fig. 11, which is a contour plot of relative
critical velocity ratio on the blade-to-blade midspan
surface viewed from an oblique angle. It is the grid
plane curvature effect which is responsible for the
illusion of a thicker boundary layer on the blade pres-
sure surface in Figs. 6, 7, 9, and 10. Figure 11 indi-
cates that this is not the case, as the suction surface
boundary layer is clearly thicker than that of the
pressure surface.

It can be seen from Fig. 11 that the flow acceler-
ates from a relative velocity ratio of about 0.3 at
inlet to approximately sonic relative velocity at the
exit. The turbulent wake behind the blade trailing
edge is characterized by the large velocity gradient in
this region. The blade wake direction follows the
blade exit angle closely. Another region of large
velocity gradients is on the blade suction surface near
the leading edge. Here the flow is rapidly expanding
and accelerating around the leading edge after stagnat-
ing on the nearby pressure surface.

A very small separation region was detected in the
nonclearance viscous solution. This region is located
at the intersection of the hub and the blade suction
surface, where the hub first begins to turn from the
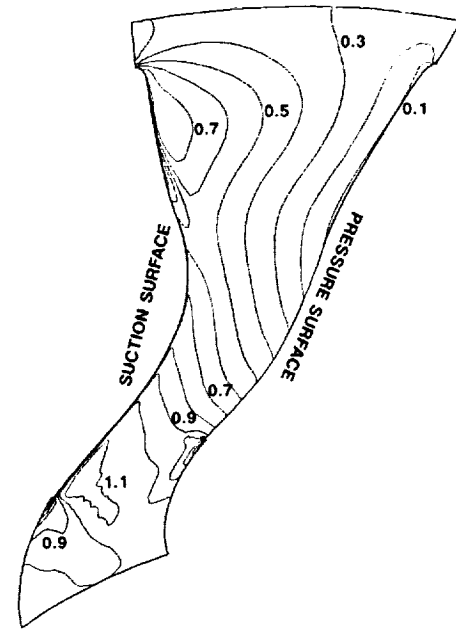radial direction. However, this separation region was

not encountered in the clearance viscous solution.
This is due to the blade hub clearance flow which
entrains the boundary layer flow in the radial portion
of the hub, and keeps the flow from separating.

Using the 5.0 pressure ratio condition, the invis-
cid code predicted a mass flow rate of 2.87 kg/s
(6.33 lb/s). The viscous nonclearance code predicted
a mass flow rate of 2.79 kg/s (6.16 lb/s), and the vis-
cous clearance code predicted a mass flow rate of
2.78 kg/s (6.12 lb/s). The experimental value was
2.86 kg/s (6.30 lb/s). This indicates that the viscous
solutions underpredicted the flow rate due to the
blockage effect of the wall boundary layers. Mass flow
rate was conserved for each of the three calculations
to within 0.5 percent from inlet to exit. Doubling
the artificial viscosity terms from the typical values
reduced the converged mass flow rate by less than
0.5 percent.

Figures 12 to 15 present computed quantities in comparison to experimental results, which are by their nature averages. In order to make this comparison, the computed local quantities must be averaged in the blade-to-blade direction. The local density, pressure, internal energy, and three components of momentum were circumferentially averaged on a flow area basis along blade-to-blade grid lines. These axisymmetric average quantities were then used to calculate any derived axisymmetric average quantities such as the total pressure, total temperature, and flow angle. These are the quantities plotted in Figs. 12 to 15.

Figure 12 compares the rotor exit swirl flow angles for the three previously discussed solutions with experimental data. The exit flow angle is defined as the angle between the absolute exit velocity and the axial direction, neglecting the radial velocity component. The direction of rotor rotation is considered positive. The inviscid solution fails to predict the local maximum at 75 percent span indicated by the data. However, the nonclearance viscous calculation does predict this maximum. This can be explained by the counterrotating vortex behavior present in the viscous solution. The fluid between the passage and scraping vortices tends to underturn; that is, its velocity in the rotational direction is greater than the main flow. This corresponds to the maxima at 75 percent span in Fig. 12. The clearance viscous solution however, does not predict this behavior as well. This is due to the tip clearance flow which dominates the scraping vortex and causes the entire region to have negative (clockwise) axial vorticity. Thus, underturning does not occur at 75 percent span, but much nearer the shroud. This effect causes the two viscous solutions to bracket the data at the shroud. Such bracketing of the data may indicate that the tip clearance in the axial portion of the rotor is overestimated in the clearance viscous solution. The tip clearance model considers the blade tip to be along a grid line. However, the grid is much denser from hub to tip in the radial portion of the rotor due to the much smaller span there. Thus, it was necessary to underpredict the clearance in the radial portion and overpredict the clearance in the axial portion to minimize the error caused by the varying clearance model. This problem was not encountered with the hub clearance, since the hub clearance is entirely in the radial region of the rotor. It is unclear why all solutions predict underturning relative to the experimental data in the 30 to 40 percent span region. Choo and Civinskas (Ref. 1) noted a similar trend in their inviscid analysis of a radial turbine for span locations less than 40 percent. This was explained by viscous effects such as boundary layer and wake development which would not be modeled by an inviscid analysis. However, the viscous and inviscid analyses in this study predict a nearly identical rotor exit flow angle in the 30 to 40 percent span range.

Figure 13 compares the rotor exit total pressures for the three solutions with experimental data. The pressures are normalized with respect to the rotor inlet total pressure. The viscous solutions correctly predict a reduction in total pressure very near the hub and shroud. This is due to the boundary layer flow near the walls. The clearance solution predicts a drop in total pressure at about 80 to 90 percent span. This may again be due to an overestimation of the tip clearance in the axial section of the rotor. However, some loss of total pressure in the shroud region is expected due to tip clearance losses.

Figure 14 compares the rotor exit total temperatures for the three solutions with experimental data. The temperatures are normalized with respect to the rotor inlet total temperature. Due to the vortex behavior and boundary layer losses present in the nonclearance viscous solution, it predicts a higher exit total temperature (higher loss) than the inviscid solution at about 80 percent span. This brings the solution closer to the data, but the average exit total temperature is still lower than the experiment. This indicates an underprediction of loss. When the clearance model is introduced, the exit total temperature again increases and corresponds more closely to the data. This implies that the clearance model produces a loss relative to the nonclearance viscous calculation.

Figure 15 compares the axisymmetric average shroud static pressures for the three solutions with experimental data. The pressures are normalized with respect to the rotor inlet total pressure. All three solutions agree well with each other. This indicates that the shroud pressure distribution is governed more by the inlet and exit boundary conditions and the rotor geometry than by viscous and clearance effects. However, the solutions differ from the data in the 0 to 50 percent meridional distance range. This is perhaps due to an inaccurate estimation of rotor pressure ratio. The exit pressure is accurately matched, as expected.

Figures 16 to 18 show the static pressures on the blade suction and pressure surfaces at the hub, midspan, and tip, respectively, for the three solutions. The hub, midspan, and tip stations are the same for each solution. The hub and tip stations were taken as the first grid points on the blade surface for the clearance solution. This corresponds to the fourth grid point from the hub and the third grid point from the tip, respectively. The pressures are normalized with respect to the rotor inlet total pressure. In the radial portion of the rotor (approximately 0 to 30 percent meridional distance) the blade loading is fairly constant from hub to tip. This is because the wheel speed does not vary from hub to tip in this portion of the rotor. However, in the axial portion of the rotor (approximately 60 to 100 percent meridional distance) the loading increases from hub to tip. This is typical axial turbine behavior, and arises due to the increase in wheel speed from hub to tip.

At the tip, the clearance viscous calculation predicts a higher loading than the nonclearance viscous calculation. To a lesser extent, this is also true in the hub clearance region. For the nonclearance viscous solution, the suction surface of the blade passes over the shroud with no leakage. Therefore the blade tip becomes a stagnation line with a static pressure equal to the relative total pressure. However, when the clearance is introduced, the blade tip is no longer a stagnation line, since there is leakage. Thus the blade suction tip static pressure is lower than the total pressure, and lower than the nonclearance value. In the inviscid solution, the shroud rotation has no effect, so as in the clearance viscous solution the suction surface tip static pressures do not reach the total pressure. It is interesting that the inviscid solution agrees with the clearance viscous solution better than the viscous nonclearance solution. This is due to the physically unrealistic condition which exists in the viscous nonclearance solution. It is physically unrealistic to assume that the fluid is bound by the no-slip condition to both the shroud and to the blade suction surface, yet flow cannot escape between the two surfaces as clearance flow. However, this is a highly localized effect, limited to a region very near the clearance. Over most of the blade surface, the clearance solution predicts a reduced loading such as that seen in the midspan plot. Thus, the overall blade loading is smaller for the clearance viscous calculation than for the nonclearance viscous calculation, as expected.
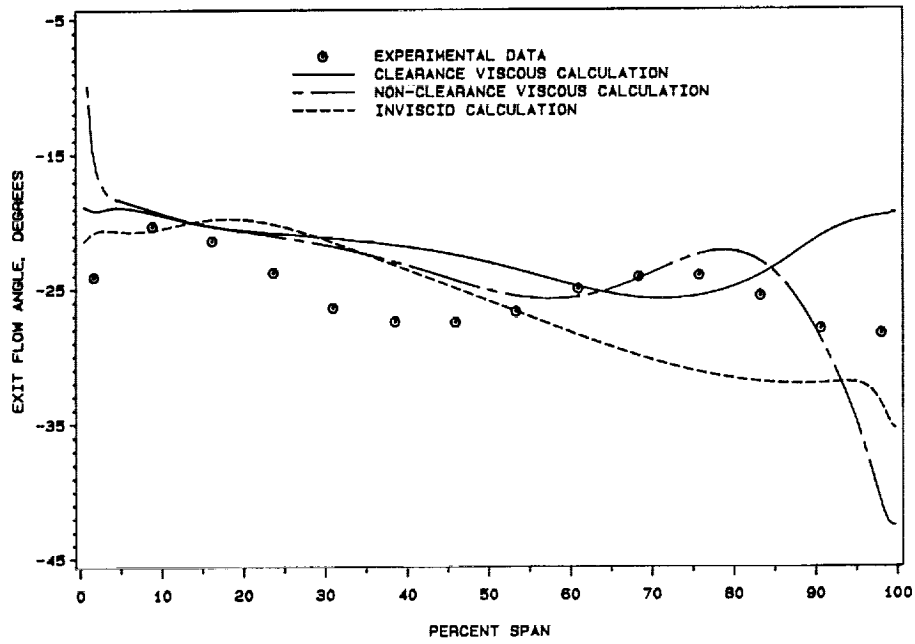
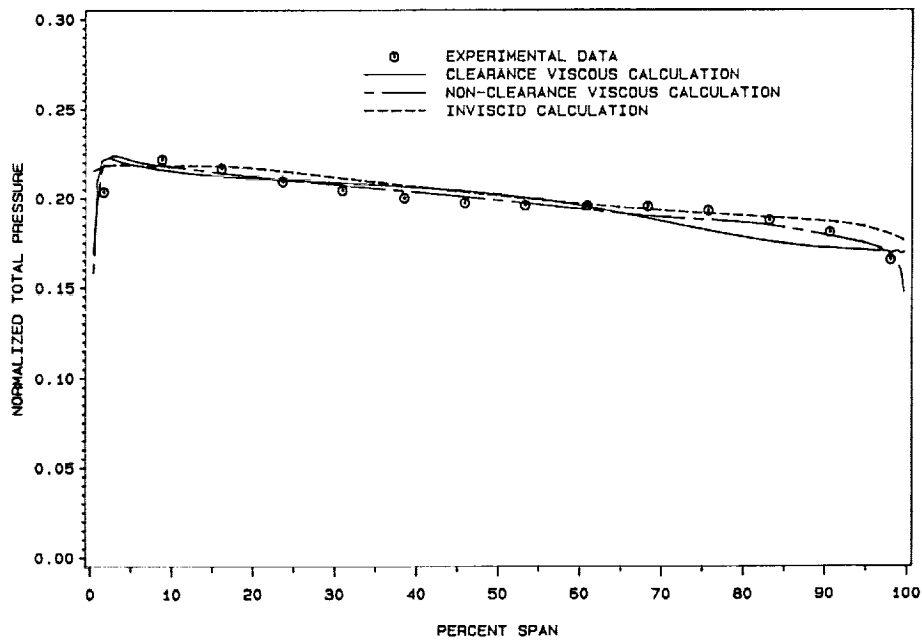**Figure 12 - Rotor exit flow angle versus percent span**

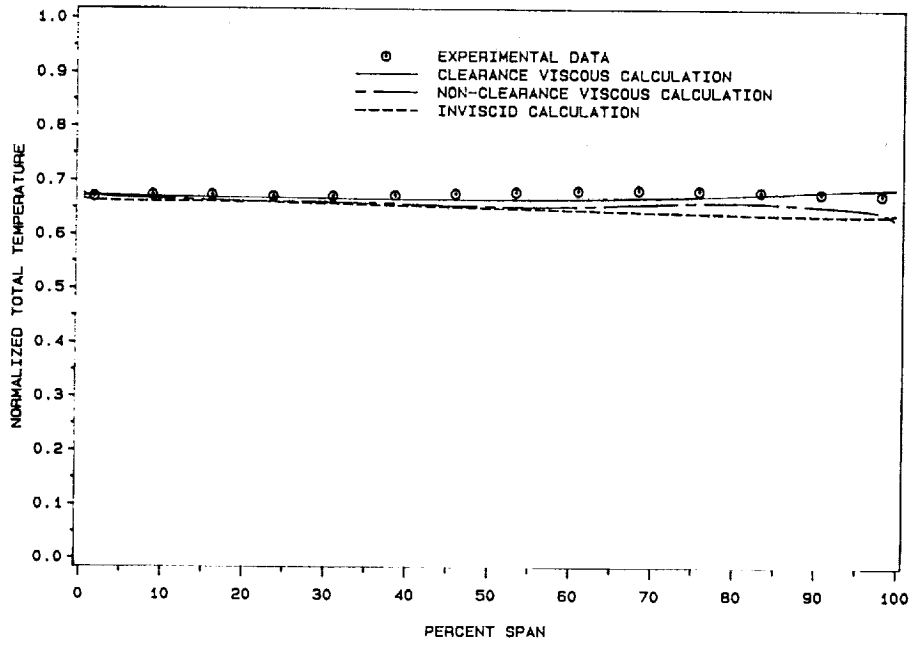**Figure 13 - Rotor exit total pressure versus percent span**

Figure 14 - Rotor exit total temperature versus percent span
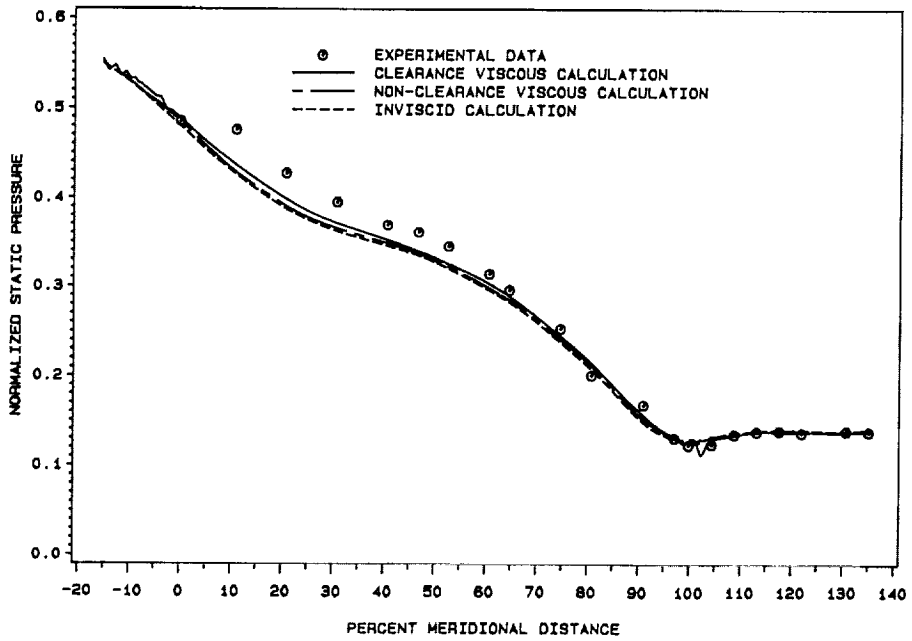

Figure 15 - Axisymmetric shroud pressure versus meridional distance
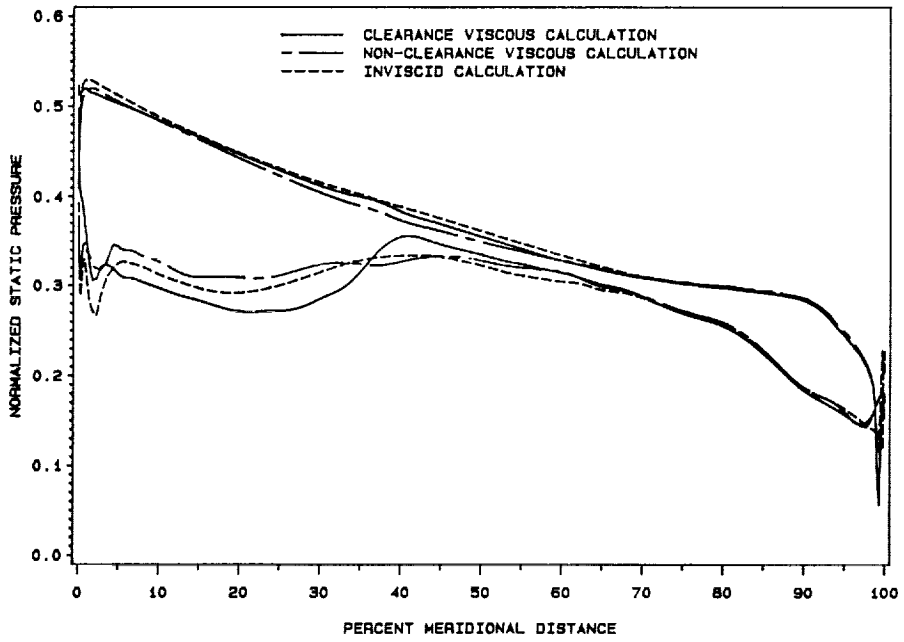
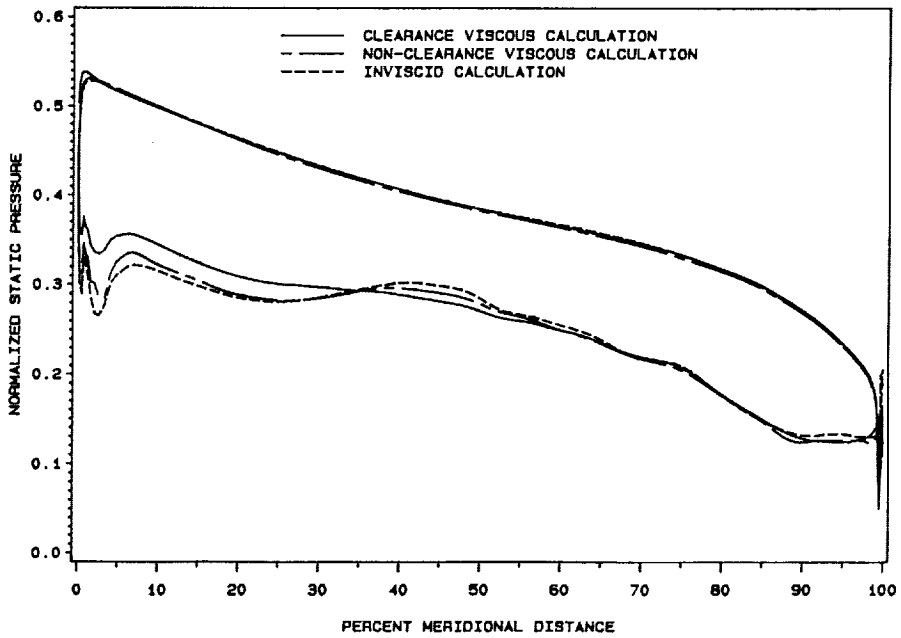9

Figure 16 - Blade loading diagram at hub

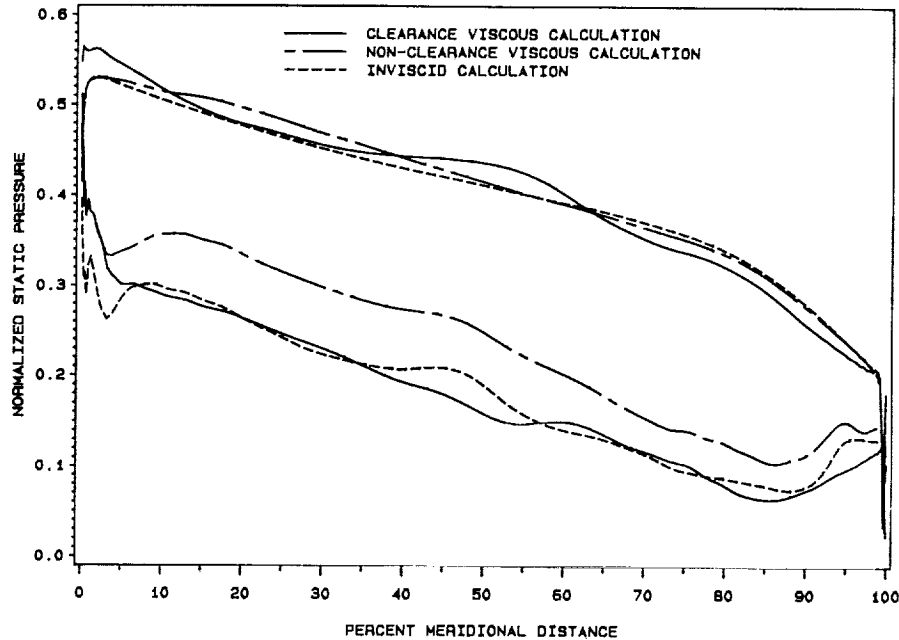Figure 17 - Blade loading diagram at midspan

Figure 18 - Blade loading diagram at tip

CONCLUDING REMARKS

The three-dimensional average passage code was modified for use with radial turbomachinery. It was applied to analyze the flow field in an advanced compact radial turbine rotor. Progressively improved computational models were employed, including an inviscid solution, a viscous solution without clearance, and a viscous solution with clearance. Comparisons of the calculated flow fields with test data showed good agreement with total pressure and total temperature, but rather poorer agreement with flow angle. The agreement with rotor exit total temperature was best for the most realistic model, namely the viscous blade clearance model. Both viscous solutions better predicted experimental trends in rotor exit flow angle than did the inviscid solution and better predicted hub and shroud effects in the rotor exit total pressure. However, the clearance viscous solution deviated from the flow angle and total pressure data near the shroud. This was perhaps due to an overestimation of tip clearance in the axial portion of the rotor. Near the midspan region the viscous clearance solution showed the poorest agreement with the measured flow angle and total pressure.

The average passage code allows for the interpretation of secondary flows. It also brings a better insight into the flow physics of turbomachinery, which is particularly complex in radial machines such as the compact radial turbine rotor. This insight can lead to an explanation of experimental trends, which makes the code a powerful new analysis tool. With experience, the knowledge of secondary flow patterns can lead to improved turbomachinery designs and increased engine efficiencies.

REFERENCES

1. Choo, Y.K. and Civinskas, K.C., 1985, "Three-Dimensional Inviscid Analysis of Radial Turbine Flow and a Limited Comparison With Experimental Data," NASA TM-87091 and USAAVSCOM TR 85-C-12.

2. Denton, J.D., 1983, "A Method of Calculating Fully Three-Dimensional Inviscid Flow Through Any Type of Turbomachine Blade Row," Aerothermodynamics of Low Pressure Steam Turbines and Condensers, Vol. 1, VKI-LS-1983-06-VOL-1, Von Karman Institute for Fluid Dynamics, Rhode-Saint-Genese, Belgium.

3. Zangeneh-Kazemi, M., Dawes, W.N. and Hawthorne, W.R., 1988, "Three Dimensional Flow in Radial-Inflow Turbines," ASME Paper 88-GT-103.

4. Adamczyk, J.J., 1985, "Model Equation for Simulating Flows in Multistage Turbomachinery," ASME Paper 85-GT-226 and NASA TM-86869.

5. Adamczyk, J.J., Mulac, R.A., and Celestina, M.L., 1986, "A Model for Closing the Inviscid Form of the Average-Passage Equation System," ASME Paper 86-GT-227.

6. Celestina, M.L., Mulac, R.A., and Adamczyk, J.J., 1986, "A Numerical Simulation of the Inviscid Flow Through a Counterrotating Propeller," Journal of Turbomachinery, Vol. 108, No. 4, pp. 187-193.

7. Katsanis, T. and McNally, W.D., 1977, "Revised FORTRAN Program for Calculating Velocities and Streamlines on the Hub-Shroud Midchannel Stream Surface of an Axial-, Radial-, or Mixed-Flow Turbomachine or Annular Duct, I - User's Manual," NASA TN-D-8430.

NASA National Aeronautics and Space Administration	Report Documentation Page	

1. Report No. NASA TM-102471	2. Government Accession No.	3. Recipient's Catalog No.
4. Title and Subtitle An Analysis of the Viscous Flow Through a Compact Radial Turbine by the Average Passage Approach		5. Report Date
		6. Performing Organization Code
7. Author(s) James D. Heidmann and Timothy A. Beach		8. Performing Organization Report No. E-5258
		10. Work Unit No. 505-05-01
9. Performing Organization Name and Address National Aeronautics and Space Administration Lewis Research Center Cleveland, Ohio 44135-3191		11. Contract or Grant No.
		13. Type of Report and Period Covered Technical Memorandum
12. Sponsoring Agency Name and Address National Aeronautics and Space Administration Washington, D.C. 20546-0001		14. Sponsoring Agency Code

15. Supplementary Notes

16. Abstract

A steady, three-dimensional viscous "average passage" computer code is used to analyze the flow through a compact radial turbine rotor. The code models the flow as spatially periodic from blade passage to blade passage. Results from the code using varying computational models are compared with each other and with experimental data. These results include blade surface velocities and pressures, exit vorticity and entropy contour plots, shroud pressures, and spanwise exit total temperature, total pressure, and swirl distributions. The three computational models used are inviscid, viscous with no blade clearance, and viscous with blade clearance. It is found that modeling viscous effects improves correlation with experimental data, while modeling hub and tip clearances further improves some comparisons. Experimental results such as a local maximum of exit swirl, reduced exit total pressures at the walls, and exit total temperature magnitudes are explained by interpretation of the flow physics and computed secondary flows. Trends in the computed blade loading diagrams are similarly explained.

17. Key Words (Suggested by Author(s)) Analysis Viscous Turbine	18. Distribution Statement Unclassified – Unlimited Subject Category 02		
19. Security Classif. (of this report) Unclassified	20. Security Classif. (of this page) Unclassified	21. No. of pages 12	22. Price* A03